RSC Advances

PAPER

View Article Online
View Journal | View Issue

Cite this: *RSC Adv.*, 2017, **7**, 30433

The synthesis and magnetic properties of $BaFe_2Se_3$ single crystals†

Juanjuan Gao,[a] Yifei Teng,[a] Wei Liu,[a] Shufan Chen,[b] Wenming Tong,[a] Min Li,[a] Xudong Zhao*[a] and Xiaoyang Liu*[a]

Received 14th March 2017
Accepted 22nd May 2017

DOI: 10.1039/c7ra03031b

rsc.li/rsc-advances

The iron selenide compound $BaFe_2Se_3$ was synthesized by a two-step high-temperature solid state method. The single-crystal X-ray determination of the prepared compound revealed a three-dimensional structure consisting of double chains of edge-sharing $FeSe_4$ tetrahedra separated by Ba^{2+}. In contrast to the case for alkali metal intercalated iron-based chalcogenides (like $K_xFe_{2-y}Se_2$), the double chains of $BaFe_2Se_3$ were cut out of the two-dimension layers. X-ray photoelectron spectroscopy measurements indicated that there existed two valence states of iron: Fe^{2+} and Fe^{3+}, which proved there were vacancies in the iron sites. In addition, the magnetic measurements demonstrated that $BaFe_2Se_3$ was antiferromagnetic and the Neel temperature of the sample was related to the average electronic spin of iron sites.

Introduction

The condensed matter theory of strongly correlated electronic systems has been established for many years, but problems have remained unanswered, the most prominent of which is to understand the mechanism of high-temperature superconductivity and the correlated phenomena such as antiferromagnetism, pseudogap and *etc.* Ever since the discovery of the high-temperature superconductivity in layered copper-based oxides,[1–7] it has been widely believed that the high superconducting transition temperature (T_C) of the copper oxides was caused by the strong electron correlation associated with the transition metal ions. Therefore, extensive efforts have been devoted to the exploration of new material systems containing transition metals other than copper,[8] which have led to the discovery of a variety of iron-based superconductors, such as the ZrCuSiAs-type LnFeAsO (Fe-1111, Ln is a rare-earth element),[9] the $ThCr_2Si_2$-type $AeFe_2As_2$ (Fe-122, Ae is an alkaline-earth element),[10] the Fe_2As-type AFeAs (Fe-111, A is Li or Na),[11] and the anti-PbO-type Fe(Se,Te) (Fe-11).[12–16] In these superconducting compounds, two-dimensional FePn or FeCh (Pn = pnictogens, Ch = chalcogens) tetrahedron layers are the most common structural components.[17–25] And for $AnFe_2X_3$ (Fe-123, An is an alkali metal or alkaline earth metal element, X is a chalcogen element),[26–31] only $BaFe_2S_3$ shows superconductivity with the critical temperature (T_C) of 14 K under the pressure of 11 GPa,[32] which is a one-dimensional quasi system. However, superconductivity in MFe_2Se_3 (M = K, Ba, and Cs) has not yet been discovered by electron or hole doping or high pressure.[33,34]

The key to study the strongly correlated electron interaction of high-temperature superconductors is to understand the superconductivity phase diagram with the change of electron or hole doping concentrations. The superconducting phase diagram mainly includes three parts: antiferromagnetic phase, superconducting phase and pseudo energy gap. The previously reported $BaFe_2Se_3$ was antiferromagnetic.[35,36] Exploring the quasi one-dimensional structure and properties of $BaFe_2Se_3$ is beneficial to study the phase diagram of iron-based chalcogenides.

In the previous literature, for $BaFe_2Se_3$, long-range antiferromagnetic order was developed at temperatures below $T_N = 256$ K[36] or $T_N = 240$ K,[37] and the short-range antiferromagnetic correlations persisted up to room temperature.[38,39] Nevertheless, the iron-deficient semi-conducting $BaFe_{1.79}Se_3$ phase did not have long-range antimagnetic order below 240 K or 256 K.[40] It indicated that the antiferromagnetic transition temperature may be related to the average electronic spin of iron sites. However, the previously reported magnetic susceptibility curve was significantly different from the standard antiferromagnetic curve because of the poor quality of the single crystals. Therefore, high-quality single crystals are needed to study the relationship between the antiferromagnetic transition temperature and the average electronic spin of iron sites.

In the previous literature, $BaFe_2Se_3$ single crystals were synthesized by one-step solid state method.[33,37,40] However, it is difficult to control the proportion of selenium of single crystals due to the volatility of selenium. In addition, in the synthetic process of $BaFe_2Se_3$, aluminum oxide crucible, carbon crucible

[a]*State Key Laboratory of Inorganic Synthesis and Preparative Chemistry, College of Chemistry, Jilin University, Changchun 130012, P. R. China. E-mail: xdzhao@jlu.edu.cn; liuxy@mail.jlu.edu.cn*

[b]*Department of Analytical Chemistry, College of Chemistry, Jilin University, Changchun 130012, P. R. China*

† CCDC 1537571. For crystallographic data in CIF or other electronic format see DOI: 10.1039/c7ra03031b

or quartz crucible was used before.[38,39] However, the reaction of carbon with iron selenide at high temperatures prohibited the formation of the product, and in the presence of alkaline earth metals, quartz crucible may undertake devitrification at high temperatures that also impedes the single crystal formation. In addition, the aluminum oxide crucible makes the single crystals difficult to be got out due to the rough and sticky surface. In contrast, boron nitride is chemical inert enough not to react with the reactants and the sample is easy to be got out. Therefore, the boron nitride crucible is a very promising tool for the synthesis of $BaFe_2Se_3$ with high-quality single crystals.

In this paper, FeSe precursor was firstly synthesized in order to avoid the volatilization of selenium and boron nitride crucible was used here. We synthesized $BaFe_2Se_3$ single crystal by a quartz tube encapsulation method successfully. And its single-crystal structure and magnetic properties were also reported, which showed a clear antiferromagnetic transition in the magnetic moment.

Results and discussion

Fig. 1(a) shows the powder XRD pattern of sample powder. The product was $BaFe_2Se_3$, which was indicated by comparing experimental data with standard JCPDS cards of no. 39-0439. The EDX spectrum of a single crystal confirmed the presence of element Ba, Fe, and Se. The average atomic ratio determined from EDX was Ba : Fe : Se = 1 : 1.89(5) : 2.99(8), close to the expected stoichiometric $BaFe_2Se_3$ ratio. And there could be vacancies in the iron sites.

The results of structural refinement and crystal data for the $BaFe_2Se_3$ single crystal collected at 296 K were presented in Tables 1 and 2. The sample crystallized in the *Pnma* space group (no. 62) with cell parameters of $a = 11.936(2)$ Å, $b = 5.4322(10)$ Å, $c = 9.1679(18)$ Å. The crystal structure of $BaFe_2Se_3$, as shown in Fig. 1(b), can be depicted as double chains of $[Fe_2Se_3]^{2-}$ formed by edge-shared $FeSe_4$ tetrahedra extending along the *b* axis, with channels occupied by Ba^{2+} cations. Compared with the Fe-122 iron based superconductors, $BaFe_2Se_3$ and $K_xFe_{2-y}Se_2$ were similar in that they could both be viewed as alternate stacking of Fe–Se layers and cations. However, for $BaFe_2Se_3$, $FeSe_4$ tetrahedra did not connect with each other along the two planar directions to form a two-dimensional layer. On the contrary, they were periodically broken along the *c* axis, and only one-dimensional double chains of edge-connected $FeSe_4$ tetrahedra along the *b* axis was shaped.

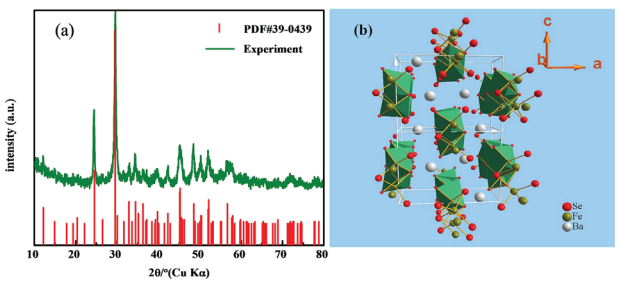

Fig. 1 (a) Powder XRD pattern of $BaFe_2Se_3$. (b) The crystal structure of $BaFe_2Se_3$.

Table 1 Single crystal data and structure refinement for $BaFe_2Se_3$ collected at 296(2) K

Empirical formula	$BaFe_{1.95}Se_3$
Wavelength, Å	0.71073
Formula weight	483.13
Lattice parameters *a*/*b*/*c*, Å	11.936(2)/5.4322(10)/ 9.1679(18)
Crystal system, space group	Orthorhombic, *Pnma*
Volume, Å^3	594.4(2)
Z	4
Density (caculated), g cm^{-3}	5.399 g cm^{-3}
θ range for data collection	2.802–24.990°
Index ranges, *h*; *k*; *l*	$-12 \le h \le +14$; $-6 \le k \le +6$; $-10 \le l \le 9$
Reflections collected	2889
Independent reflections	570
Completeness to max 2θ, %	97.8
Data/parameters	570/34
Goodness-of-fit on F^2	1.028
Final *R* indices ($I > 2\sigma(I)$)	$R_1 = 0.0433$, $WR_2 = 0.1063$
R indices (all data)	$R_1 = 0.0452$, $WR_2 = 0.1072$
Largest diff. peak/hole, (Å^3)$^{-1}$	1.535/−1.886

Table 2 Atomic coordinates and equivalent isotropic displacement parameters (Ueq) for $BaFe_2Se_3$ single crystal collected at 296(2) K. Ueq is defined as one third of the trace of the orthogonalized Uij tensor

	Site	*x*	*y*	*z*	Ueq (Å^2)
Ba	4c	0.3152(1)	1/4	0.4806	0.024(1)
Fe	8d	0.4944(1)	−0.0004(3)	0.1473(2)	0.013(1)
Se1	4c	0.3587(1)	−1/4	0.2712(2)	0.020(1)
Se2	4c	0.3721(1)	1/4	−0.0087(2)	0.016(1)
Se3	4c	0.6012(2)	1/4	0.3132(2)	0.023(1)

Table 3 The bond angles (°) for $BaFe_2Se_3$ synthesized (left) and $BaFe_2Se_3$ reported (right). The angular data of $BaFe_2Se_3$ reported was obtained according to the atomic positions in the literature

	$BaFe_2Se_3$ synthesized	$BaFe_2Se_3$ reported
Se1–Fe1–Se3	112.22(9)	111.98(2)
Se1–Fe1–Se2	111.85(7)	111.65(0)
Se3–Fe1–Se2	107.25(8)	107.57(2)
Se1–Fe1–Se2	100.83(8)	100.83(5)
Se3–Fe1–Se2	111.72(7)	111.73(5)
Se2–Fe1–Se2	113.03(7)	113.08(6)

The bond lengths and bond angles were shown in Tables 3 and 4. We observed that the four distinct Fe–Se distances were in the range of 2.398(2)–2.455(2) Å, and tetrahedral angles around iron were in the range of 100.83(8)–113.03(7)°, which were within the normal range for iron selenides. All the distances and angles for $BaFe_2Se_3$ matched well with previous literature reports.[39] At 296 K, the Ba–Se interatomic distances ranged from 3.366(3) to 3.743(2) Å. Within a double chain, the

Table 4 Interatomic distances in the compound $BaFe_2Se_3$

Atom1–atom2	Distance (Å)	Atom1–atom2	Distance (Å)
Ba1–Se1	3.3663	Fe1–Se2	2.448(2)
Ba1–Se1	3.378(2)	Fe1–Se2	2.455(2)
Ba1–Se2	3.5194	Fe1–Se3	2.406(2)
Ba1–Se3	3.4563	Fe1–Fe1	2.705(3)
Ba1–Se3	3.712(2)	Fe1–Fe1	2.712(3)
Ba1–Se3	3.743(2)	Fe1–Fe1	2.721(3)
Fe1–Se1	2.398(2)		

Fe–Fe distance in adjacent chains was 2.705(3) Å, whereas within a single chain, there existed two kinds of Fe–Fe distances with the values of 2.712(3) and 2.721(3) Å respectively, which were arranged alternately. These Fe–Fe distance values were in the range of 2.616(2)–2.832(2) Å (presumably the range of the distances between two Fe atoms) which was reported by Caron *et al.*[36] As shown in Table 3, compared with the previous report,[39] the bond angles of Se1–Fe1–Se3 and Se1–Fe1–Se2 increased by about 0.24(7)° and 0.20(7)°, respectively. Instead, the bond angle of Se2–Fe1–Se3 decreased by 0.31(4)°. It indicated that, in contrast to bond lengths and bond angles in the literature,[39] there was a slight distortion in the crystal lattice, which might induce the changes of antiferromagnetic transition temperature.

As shown in Fig. 2, the powder XRD pattern of $BaFe_2Se_3$ was consistent with the simulated XRD pattern based on the single-crystal structural analysis, indicating that they held the same structure.

Temperature dependence of the magnetization $M(T)$ of $BaFe_2Se_3$ single crystal from 2 to 300 K under a magnetic field of 10 Oe was shown in Fig. 3(a). The magnetization curves showed significant antiferromagnetic characteristics and the magnetic moments showed a maximum around 140 K, which represented the Neel temperature (T_N). In addition, there was a drop of magnetic moment at about 11 K for the ZFC measurement. This was also observed in a previous paper[37] and might corresponded to the superconducting transition.

Nevertheless, other studies on $BaFe_2Se_3$ indicated that there was no superconductive response over the entire temperature range of 1.8 K to 300 K.[36] Therefore, the superconducting

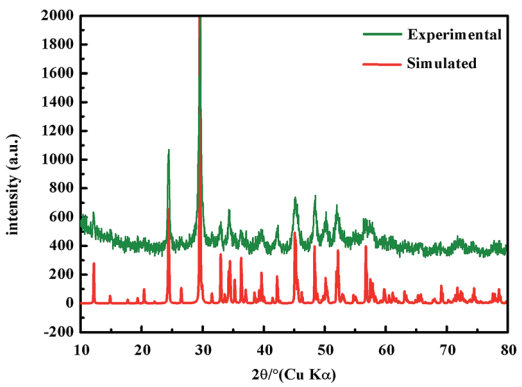

Fig. 2 Simulated and experimental powder XRD patterns of $BaFe_2Se_3$.

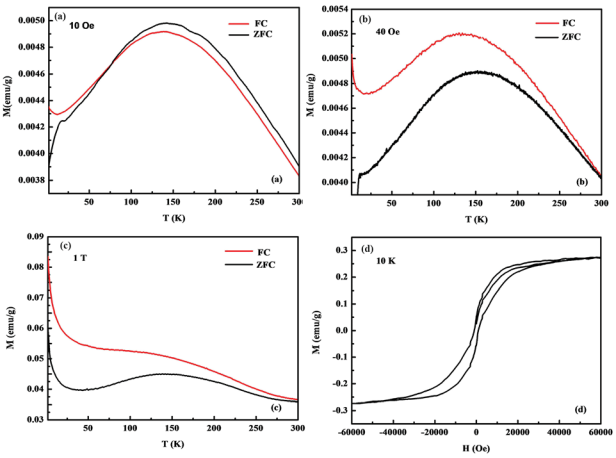

Fig. 3 Temperature dependence of magnetization for $BaFe_2Se_3$ under ZFC (black solid line) and FC (red solid line) modes with the applied field (a) H = 10 Oe (b) H = 40 Oe (c) H = 1 T. (d) Magnetization hysteresis loop $M(H)$ at 10 K.

transition in our sample should be extrinsic and coming from residual β-FeSe. From the FC curve, we observed that there was an upturn at around 30 K, which may be attributed to the spin-glass transition.[33,34] Compared with the previous work,[36,38] the magnetization curves in this work were more ideal, which meaned that we might have got high-quality single crystals.

From the magnetic hysteresis loop $M(H)$ at 10 K, as shown in Fig. 3(d), ferromagnetism was observed in the sample, which was probably because that there existed a tiny amount of ferromagnetic impurity Fe_7Se_8 [39] or the average electronic spin of iron sites, that was, the valance state of iron ion had fluctuated.[42]

Compared with previously reported 256 K or 240 K,[36,37] the Neel temperature of our sample was much lower, perhaps due to the change of the average electronic spin in the iron sites. To test this hypothesis, we investigated their association. The average electronic spin of iron sites can be changed by doping cobalt in $BaFe_2Se_3$, which has been reported in the previous literature.[33] According to the doping concentrations of cobalt, we calculated the average electronic spin of iron sites, and then summed up the relationship between the Neel temperature and the average electronic spin of the iron sites, which was shown in Fig. 5. On the other hand, the changes of the valence state of iron might also lead to the changes of the average electronic spin of iron sites.[43] In order to verify the supposition, the valence state of iron ion was determined by XPS analysis. Fig. 4 showed the Fe 2p XPS spectra of $BaFe_2Se_3$ sample taken at 300 K. The peaks centered at 723.780 eV and 710.900 eV could be assigned to the binding energy of Fe^{2+} 2p1/2 and Fe^{2+} 2p3/2. The peaks centered at 720.200 eV and 707.600 eV could be assigned to the binding energy of Fe^{3+} 2p1/2 and Fe^{3+} 2p3/2. These results indicated that iron ion in $BaFe_2Se_3$ could only exist as Fe^{2+} and Fe^{3+}. According to the result of XPS measurement, the area ratio of Fe^{2+} and Fe^{3+} was about 4.4753, which indicated that the molar ratio of Fe^{2+} and Fe^{3+} was 4.4753. Based on the conservation of charges, the composition of the sample was

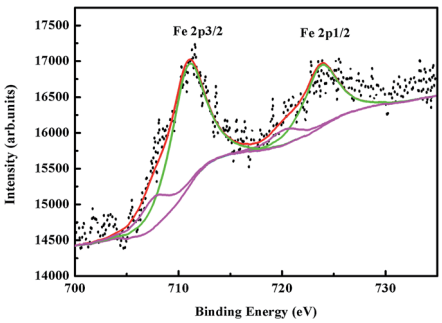

Fig. 4 XPS spectra of iron of $BaFe_2Se_3$.

$BaFe_{1.83}Se_3$, close to the atomic ratio determined from EDS. According to the results of EDS and XPS measurements and assuming that Fe^{2+} and Fe^{3+} were in the high spin configuration, we have obtained that the average electronic spin of iron sites was about 3.9526 μ_B. The calculation formula is presented: $X/2(x\mu_{Fe^{2+}} + 1\mu_{Fe^{3+}})/(x + 1)$. X is the molar content of iron in the single crystal. x is the molar ratio of Fe^{2+} to Fe^{3+}. $\mu_{Fe^{2+}}$ is the magnetic moment of Fe^{2+}. $\mu_{Fe^{3+}}$ is the magnetic moment of Fe^{3+}. For our sample, $X = 1.89$, $x = 4.4753$: 1, $\mu_{Fe^{2+}} = 4\ \mu_B$, $\mu_{Fe^{3+}} = 5\ \mu_B$.

In order to investigate the magnetism, we increased the magnetic field. The temperature dependence of magnetization $M(T)$ of $BaFe_2Se_3$ single crystal from 2 to 300 K under a magnetic field of 40 Oe and 1 T were measured, as shown in Fig. 3(b) and (c). We found that the antiferromagnetic transition temperature (T_N) remained unchanged. Additionally, from the FC curve, we observed that, as the magnetic field intensity increased, the magnetic moment was also increased below the temperature of around 30 K, which was the typical spin-glass state.

From the results of temperature dependences of magnetization $M(T)$, the Neel temperature was about 140 °C, which almost corresponded with the relationship between the antiferromagnetic transition temperature and the average electronic spin of iron sites. In addition, by taking advantage of the similar method, we have also summarized the average electronic spin of iron sites dependence of spin-glass transition temperature (T_f), which confirmed that our result was almost consistent with it (see Fig. 5).

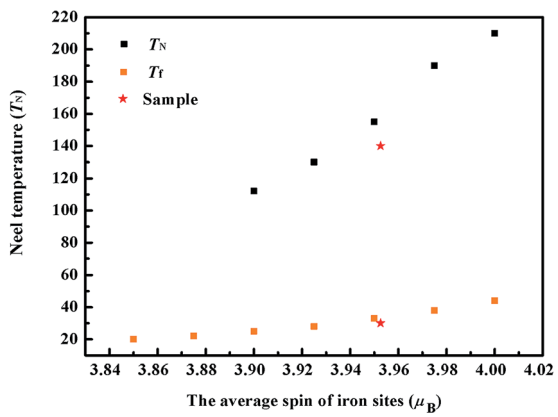

Fig. 5 The average electronic spin of iron sites dependence of antiferromagnetic transition temperature and spin-glass transition temperature for $BaFe_2Se_3$, according to Co-doped ternary compound $Ba(Fe_{1-x}Co_x)_2Se_3$. The red star represents our sample.

Experimental section

Synthesis of $BaFe_2Se_3$

Single crystals of $BaFe_2Se_3$ were grown from the melt by self-flux solid-state reaction method. β-FeSe was firstly synthesized as a precursor by reacting high purity (at least 99.99%, Alfa) iron powder with selenium powder at 410 °C for 24 h.[41] For the single-crystal synthesis, Ba pieces and β-$FeSe_{0.97}$ powder were put into a boron nitride crucible in the molar ratio of 1 : 2. The boron nitride crucible was then sealed into a double-wall evacuated quartz tube which was evacuated. The quartz tube was annealed at 1150 °C for over 2 h for homogenization. All preparations were performed in a glovebox to avoid air. Afterwards, the melt was cooled down to 750 °C at the rate of 5 °C h^{-1}, and then to room temperature at the rate of 200 °C h^{-1}. Well-formed black crystal rods of 5.8 mm diameter (the inside diameter of the boron nitride crucible) were obtained which could be easily cleaved into plates with flat shiny surfaces.

Characterization of $BaFe_2Se_3$

Powder X-ray diffraction (XRD) data were collected at room temperature using a Rigaku D/Max 2550 V/PC X-ray diffractometer with graphite-monochromated Cu Kα radiation (λ = 0.15418 nm) at 50 kV and 200 mA. The average stoichiometry was determined by examination of multiple points using an energy dispersive X-ray spectroscopy (EDX) in a JEOL JSM-6700F scanning electron microscope. The valence states of the sample were determined by X-ray photoelectron spectroscopy (XPS, ESCALAB250, USA) analysis. Magnetism measurements were done with a superconducting quantum interference device (Quantum Design, SQUID) magnetometer from 2 to 300 K in the zero-field cooled (ZFC) and field-cooling (FC) modes. Magnetic hysteresis loop $M(H)$ was conducted at 10 K.

Single-crystal structural analysis of $BaFe_2Se_3$

Suitable single crystal was selected for single-crystal XRD analysis. Intensity data were collected at a temperature of 296 K on a Bruker SMART APEX 2 micro-focused diffractometer using graphite-monochromated Mo Kα radiation (λ = 0.71073 nm) at 50 kV and 0.6 mA. Data processing was accomplished with the APEX 2 processing program. The structure was solved by direct method and refined by full-matrix least-squares technique with the SHELXTL crystallographic software package.

Conclusions

A novel two-step solid-state method to synthesize $BaFe_2Se_3$ (Fe-123) with high-quality single crystal growth was reported here. The crystal structure was similar to that of the analogous alkali metal intercalated chalcogenides, with the difference being the one-dimensional arrangement of the edge-sharing $FeSe_4$ tetrahedra creating double chains running along the *b*-axis. The

sample was antiferromagnetic with the Neel temperature of around 140 K, much lower than the reported transition temperature (T_N = 256 K or 240 K). The spin-glass transition temperature was found to be about 30 K. On the other hand, we summarized the average electronic spin of iron sites dependence of the Neel temperature or the spin-glass transition temperature, which was beneficial to understand the mechanism of high-temperature superconductors.

Acknowledgements

We greatly acknowledge financial support from the National Natural Science Foundation of China (No. 21371068 and 21271082).

Notes and references

1 P. A. Lee, N. Nagaosa and X. G. Wen, *Rev. Mod. Phys.*, 2006, **78**, 17–85.
2 J. G. Bednorz and K. A. Müller, *Z. Phys. B: Condens. Matter*, 1986, **64**, 189–193.
3 M. Enisz, E. Kristof-Mako and D. Oravetz, *J. Eur. Ceram. Soc.*, 2007, **27**, 1105–1111.
4 Z. Chen, J. Zhang, Y. Su, Y. Xue and S. Cao, *Phys. C*, 2006, **434**, 161–166.
5 M. T. D. Orlando, C. A. C. Passos, J. L. Passamai Jr, E. F. Medeiros, C. G. P. Orlando, R. V. Sampaio, H. S. P. Correa, F. C. L. de Melo, L. G. Martinez and J. L. Rossi, *Phys. C*, 2006, **434**, 53–61.
6 C. Stari, A. Moreno-Gobbi, A. W. Mombru, S. Sergeenkov, A. J. C. Lanfredi, C. A. Cardoso and F. M. Araujo-Moreira, *Phys. C*, 2005, **433**, 50–58.
7 X. Zhao, G. Yu, Y. C. Cho, G. Chabot-Couture, N. Barišić, P. Bourges, N. Kaneko, Y. Li, L. Lu, E. M. Motoyama, O. P. Vajk and M. Greven, *Adv. Mater.*, 2006, **18**, 3243–3247.
8 Y. Kamihara, H. Hiramatsu, M. Hirano, R. Kawamura, H. Yanagi, T. Kamiya and H. Hosono, *J. Am. Chem. Soc.*, 2006, **128**, 10012–10013.
9 Z. A. Ren, W. Lu, J. Yang, W. Yi, X. L. Shen, Z. C. Li, G. C. Che, X. L. Dong, L. L. Sun and F. Zhou, *Chin. Phys. Lett.*, 2008, **25**, 2215.
10 M. Rotter, M. Tegel and D. Johrendt, *Phys. Rev. Lett.*, 2008, **101**, 107006.
11 X. C. Wang, Q. Q. Liu, Y. X. Lv, W. B. Gao, L. X. Yang, R. C. Yu, F. Y. Li and C. Q. Jin, *Solid State Commun.*, 2008, **148**, 538–540.
12 F. C. Hsu, J. Y. Luo, K. W. Yeh, T. K. Chen, T. W. Huang, P. M. Wu, Y. C. Lee, Y. L. Huang, Y. Y. Chu, D. C. Yan and M. K. Wu, *Proc. Natl. Acad. Sci. U. S. A.*, 2008, **105**, 14262–14264.
13 E. Pomjakushina, K. Conder, V. Pomjakushin, M. Bendele and R. Khasanov, *Phys. Rev. B: Condens. Matter Mater. Phys.*, 2009, **80**, 024517.
14 R. Khasanov, M. Bendele, K. Conder, H. Keller, E. Pomjakushina and V. Pomjakushin, *New J. Phys.*, 2010, **12**, 073024.
15 B. H. Mok, S. M. Rao, M. C. Ling, K. J. Wang, C. T. Ke, P. M. Wu, C. L. Chen, F. C. Hsu, T. W. Huang, J. Y. Luo, D. C. Yan, K. W. Ye, T. B. Wu, A. M. Chang and M. K. Wu, *Cryst. Growth Des.*, 2009, **9**, 3261–3264.
16 S. Margadonna, Y. Takabayashi, Y. Ohishi, Y. Mizuguchi, Y. Takano, T. Kagayama, T. Nakagawa, M. Takata and K. Prassides, *Phys. Rev. B: Condens. Matter Mater. Phys.*, 2009, **80**, 064506.
17 S. Medvedev, T. M. McQueen, I. A. Troyan, T. Palasyuk, M. I. Eremets, R. J. Cava, S. Naghavi, F. Casper, V. Ksenofontov, G. Wortmann and C. Felser, *Nat. Mater.*, 2009, **8**, 630–633.
18 J. Guo, S. Jin, G. Wang, S. Wang, K. Zhu, T. Zhou, M. He and X. Chen, *Phys. Rev. B: Condens. Matter Mater. Phys.*, 2010, **82**, 180520(R).
19 Y. Kamihara, T. Watanabe, M. Hirano and H. Hosono, *J. Am. Chem. Soc.*, 2008, **130**, 3296–3297.
20 A. F. Wang, J. J. Ying, Y. J. Yan, R. H. Liu, X. G. Luo, Z. Y. Li, X. F. Wang, M. Zhang, G. J. Ye, P. Cheng, Z. J. Xiang and X. H. Chen, *Phys. Rev. B: Condens. Matter Mater. Phys.*, 2011, **83**, 060512(R).
21 A. Krzton-Maziopa, Z. Shermadini, E. Pomjakushina, V. Pomjakushin, M. Bendele, A. Amato, R. Khasanov, H. Luetkens and K. Conder, *J. Phys.: Condens. Matter*, 2011, **23**, 052203.
22 C. H. Li, B. Shen, F. Han, X. Y. Zhu and H. H. Wen, *Phys. Rev. B: Condens. Matter Mater. Phys.*, 2011, **83**, 184521.
23 H. D. Wang, C. H. Dong, Z. J. Li, Q. H. Mao, S. S. Zhu, C. M. Feng, H. Q. Yuan and M. H. Fang, *Europhys. Lett.*, 2011, **93**, 47004.
24 J. J. Ying, X. F. Wang, X. G. Luo, A. F. Wang, M. Zhang, Y. J. Yan, Z. J. Xiang, R. H. Liu, P. Cheng, G. J. Ye and X. H. Chen, *Phys. Rev. B: Condens. Matter Mater. Phys.*, 2011, **83**, 212502.
25 M. H. Fang, H. D. Wang, C. H. Dong, Z. J. Li, C. M. Feng, J. Chen and H. Q. Yuan, *Europhys. Lett.*, 2011, **94**, 27009.
26 M. Wang, M. Yi, S. Jin, H. Jiang, Y. Song, H. Luo, A. D. Christianson, C. Dela Cruz, E. Bourret-Courchesne, D. X. Yao, D. H. Lee and R. J. Birgeneau, *Phys. Rev. B*, 2016, **94**, 041111(R).
27 F. Du, K. Ohgushi, Y. Nambu, T. Kawakami, M. Avdeev, Y. Hirata, Y. Watanabe, T. J. Sato and Y. Ueda, *Phys. Rev. B: Condens. Matter Mater. Phys.*, 2012, **85**, 214436.
28 S. Dong, J. M. Liu and E. Dagotto, *Phys. Rev. Lett.*, 2014, **113**, 187204.
29 M. T. Suzuki, R. Arita and H. Ikeda, *Phys. Rev. B: Condens. Matter Mater. Phys.*, 2015, **92**, 085116.
30 Y. Hirata, S. Maki, J. Yamaura, T. Yamauchi and K. Ohgushi, *Phys. Rev. B: Condens. Matter Mater. Phys.*, 2015, **92**, 205109.
31 T. Yamauchi, Y. Hirata, Y. Ueda and K. Ohgushi, *Phys. Rev. Lett.*, 2015, **115**, 246402.
32 H. Takahashi, A. Sugimoto, Y. Nambu, T. Yamauchi, Y. Hirata, T. Kawakami, M. Avdeev, K. Matsubayashi, F. Du, C. Kawashima, H. Soeda, S. Nakano, Y. Uwatoko, Y. Ueda, T. J. Sato and K. Ohgushi, *Nat. Mater.*, 2015, **14**, 1008–1012.

33 F. Du, Y. Hirata, K. Matsubayashi, Y. Uwatoko, Y. Ueda and K. Ohgushi, *Phys. Rev. B: Condens. Matter Mater. Phys.*, 2014, **90**, 085143.

34 J. M. Caron, J. R. Neilson, D. C. Miller, K. Arpino, A. Llobet and T. M. McQueen, *Phys. Rev. B: Condens. Matter Mater. Phys.*, 2012, **85**, 180405(R).

35 M. Mourigal, S. Wu, M. B. Stone, J. R. Neilson, J. M. Caron, T. M. McQueen and C. L. Broholm, *Phys. Rev. Lett.*, 2015, **115**, 047401.

36 J. M. Caron, J. R. Neilson, D. C. Miller, A. Llobet and T. M. McQueen, *Phys. Rev. B: Condens. Matter Mater. Phys.*, 2011, **84**, 180409(R).

37 A. Krzton-Maziopa, E. Pomjakushina, V. Pomjakushin, D. Sheptyakov, D. Chernyshov, V. Svitlyk and K. Conder, *J. Phys.: Condens. Matter*, 2011, **23**, 402201.

38 H. Lei, H. Ryu, A. I. Frenkel and C. Petrovic, *Phys. Rev. B: Condens. Matter Mater. Phys.*, 2011, **84**, 214511.

39 Y. Nambu, K. Ohgushi, S. Suzuki, F. Du, M. Avdeev, Y. Uwatoko, K. Munakata, H. Fukazawa, S. Chi, Y. Ueda and T. J. Sato, *Phys. Rev. B: Condens. Matter Mater. Phys.*, 2012, **85**, 064413.

40 B. Saparov, S. Calder, B. Sipos, H. Cao, S. Chi, D. J. Singh, A. D. Christianson, M. D. Lumsden and A. S. Sefat, *Phys. Rev. B: Condens. Matter Mater. Phys.*, 2011, **84**, 245132.

41 J. Janaki, T. Geetha-Kumary, A. Mani, S. Kalavathi, G. V. R. Reddy, G. V. Narasimha Rao and A. Bharathi, *J. Alloys Compd.*, 2009, **486**, 37–41.

42 D. P. Nortona and S. J. Pearton, *Appl. Phys. Lett.*, 2003, **82**, 239–241.

43 K. Komędera, A. K. Jasek, A. Błachowski, K. Ruebenbauer, M. Piskorz, J. Żukrowski, A. Krztoń-Maziopa, E. Pomjakushina and K. Conder, *Solid State Commun.*, 2015, **207**, 5–8.

